Multiscale superpixelwise prophet model for noise-robust feature extraction in hyperspectral images. [Dataset]

MA, P., REN, J., SUN, G., ZHAO, H., JIA, X., YAN, Y. and ZABALZA, J.

2023

Supplementary Materials

Multiscale Superpixelwise Prophet Model for Noise-Robust Feature Extraction in Hyperspectral Images

Ping Ma, Jinchang Ren, *Senior Member*, *IEEE*, Genyun Sun, *Member*, *IEEE*, Huimin Zhao, Xiuping Jia, *Fellow*, *IEEE*, Yijun Yan, and Jaime Zabalza

Figures

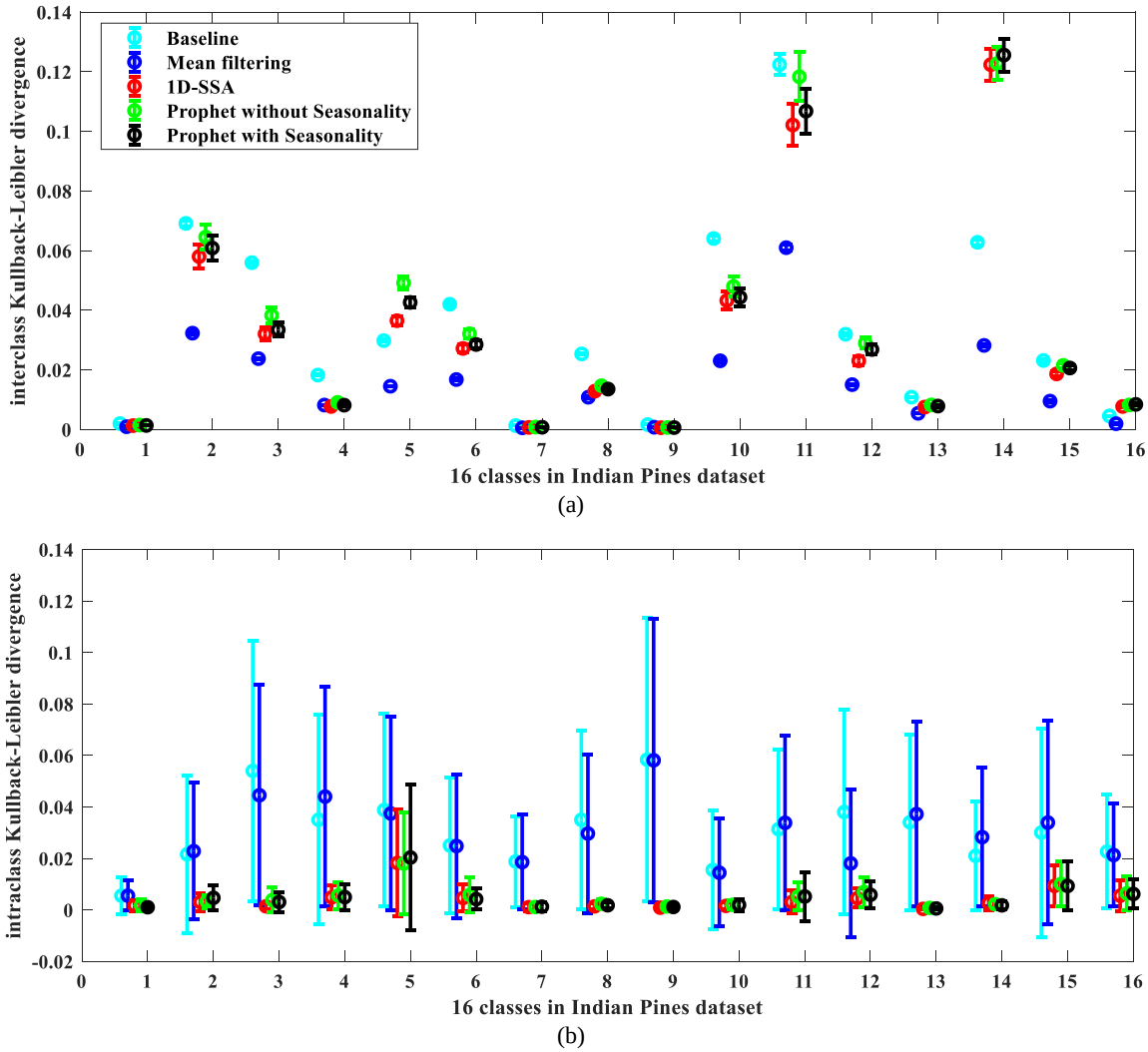

Fig. S1. The Kullback-Leibler divergence of classes in Indian Pines dataset: (a) interclass Kullback-Leibler divergence, (b) intraclass Kullback-Leibler divergence.

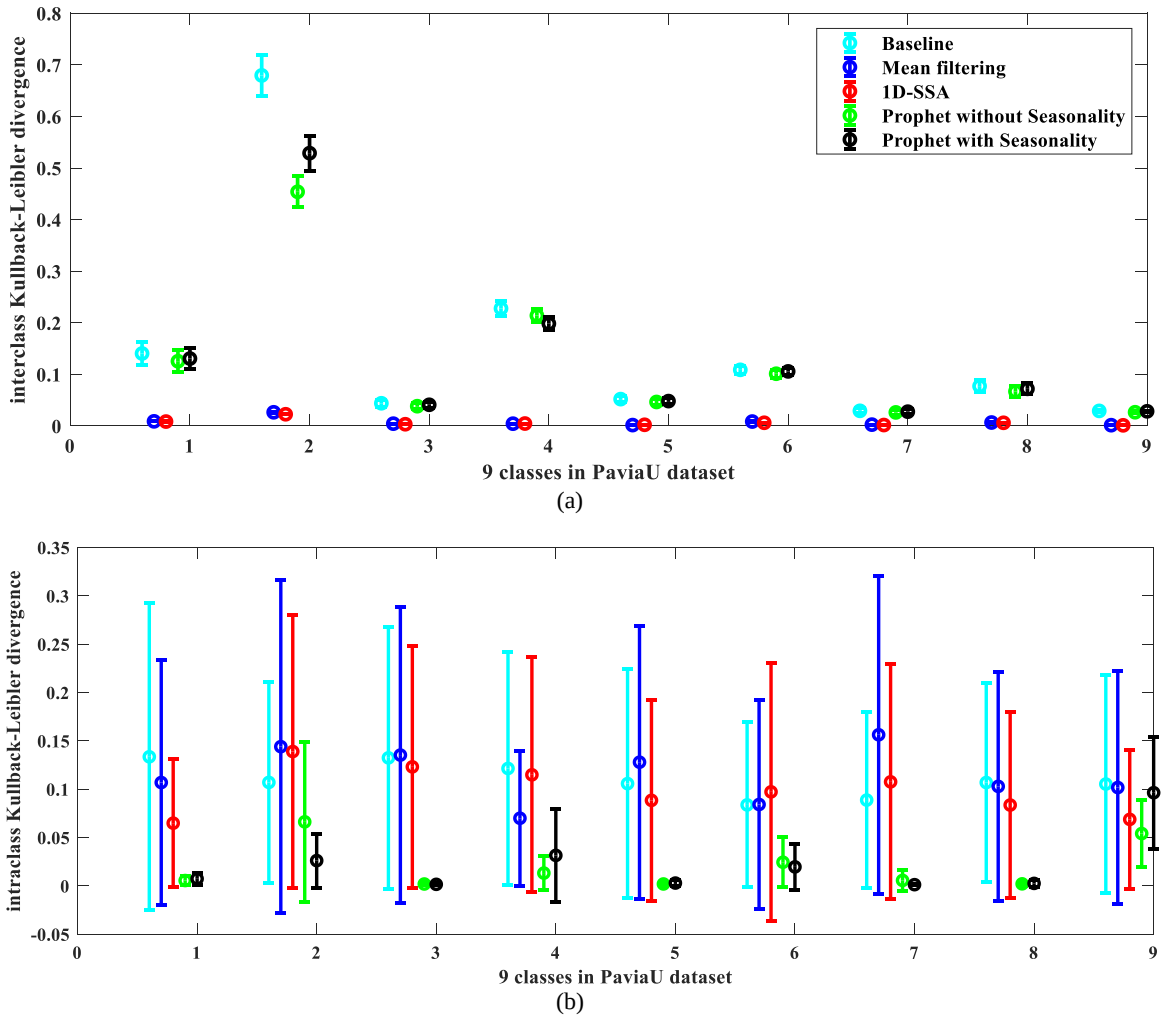

Fig. S2. The Kullback-Leibler divergence of classes in PaviaU dataset: (a) interclass Kullback-Leibler divergence, (b) intraclass Kullback-Leibler divergence.

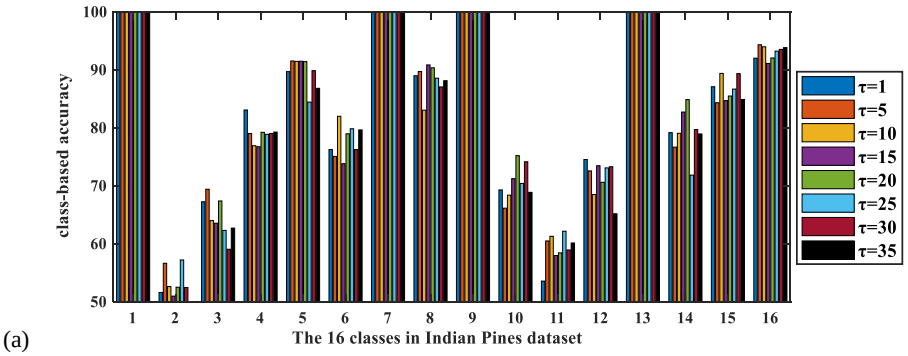

(a)

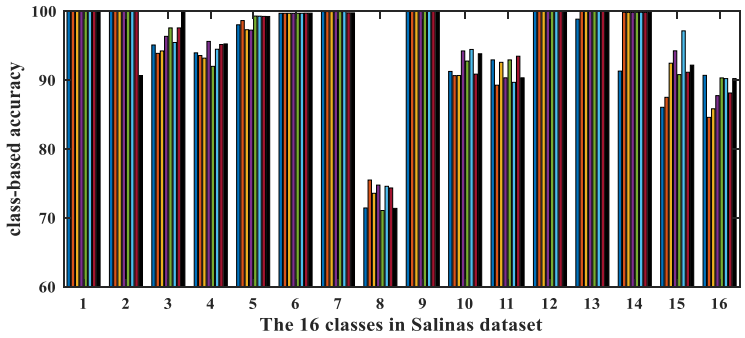

(b)

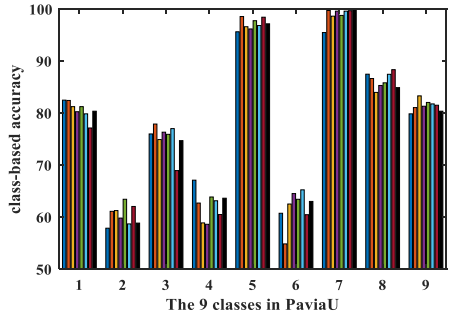

(c)

Fig. S3. The effect of the parameter τ of MSPM to (a) class-based classification accuracy on datasets of Indian Pines (b) Salinas and (c) PaviaU.

As seen in Fig. S4, with the introduced spatial information, SMLR-SpATV produces much smoother results as shown in Figs. S4 (c-d). However, the three classes *Corn-no till*, *Soybeans-min till* and *Soybeans-no till* are largely misclassified with each other as highlighted in magenta circles. Though SMLR-SpATV performs slightly better on uncorrected datasets as shown in Fig. S4 (c), it fails to preserve detailed structures and fine object boundaries. In particular, several regularly shaped land covers are distorted due to the incorrect boundaries. With further introduced superpixel segmentation, MSP-SVMsub has produced improved object boundaries, owing mainly to the homogeneous regions produced by SLIC. However, there are still several misclassified regions, especially in the *Soybeans-min till* and *Soybeans-no till* classes as highlighted in Figs. S4 (e)-(f). This may be due to improper scale values used in multiscale superpixeling, owing to noise caused high intra-variations within the land cover classes. Comparing the classification maps between Figs. S4 (e) and (f), MSP-SVMsub achieves better results on corrected dataset, whilst the 2D-MSSP obtain better classification maps than SMLR-SpATV and MSP-SVMsub as shown in Fig. S4 (g) and (h). There are still misclassifications between classes of *Corn-no till*, *Soybeans-min till* and *Soybeans-no till.* On the corrected dataset, the misclassifications between classes *Corn-no till*, *Soybeans-min till* and *Wheat* are distinct. As for our MSPM, it has produced much smoother and accurate maps and more homogeneous regions compared to all others. As highlighted in black circles in Figs. S4 (i)-(j), the complex objects with high intra-class variations can still be correctly classified by MSPM. Here, MSPM performs much better on uncorrected data when discriminating *Soybeans-min till* and *Soybeans-no till.* These visual results are consistent with the quantitative results in Table III, which has validated again the efficacy of our MSPM in noise-robust feature mining and HSI classification.

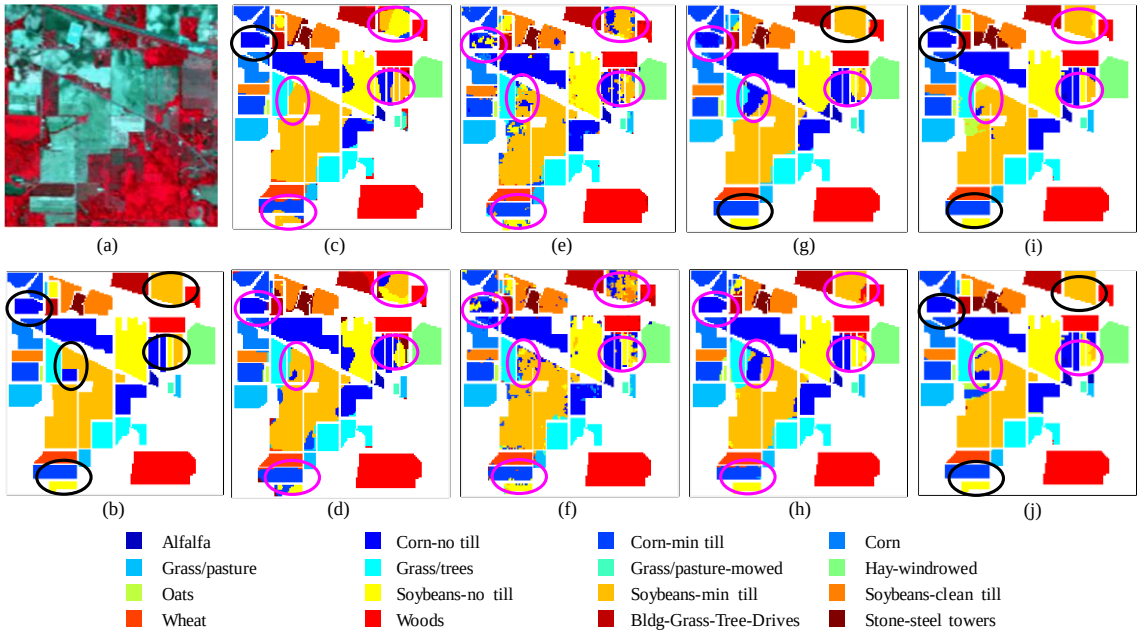

Fig. S4. Classification maps on the Indian Pines data (20 samples per class): (a) False colour image (R: 831nm, G: 657nm, B: 557nm), (b) Ground truth in 16 classes, (c) SMLR-SpATV on uncorrected data, (d) SMLR-SpATV on corrected data, (e) MSP-SVMsub on uncorrected data, (f) MSP-SVMsub on corrected data, (g) 2D-MSSP on uncorrected data, (h) 2D-MSSP on corrected data, (i) MSPM on uncorrected data and (j) MSPM on corrected data.

Regarding the classification maps in Fig. S5, it is obvious that the proposed MSPM algorithm can generate the smoothest results with a higher geometric fidelity and more accurate boundaries on the uncorrected dataset. As for the land cover classes with a high spectral and spatial similarity, such as *Vinyard untrained* and *Grapes untrained*, all approaches have difficulty to differ in between on both corrected and uncorrected datasets, as highlighted by magenta circles in Figs. S5 (c)-(j). The 2D-MSSP and the proposed MSPM show much better performance, seen in black circles in Fig. S5 (g)-(i). Besides, the misclassification between the *Corn senesced green weeds* and *Lettuce romaine 7wk* by SMLR-SpATV, MSP-SVMsub and 2D-MSSP in Figs. S5 (c)-(h) are significantly improved.

When comparing the classification maps between Figs. S5 (c) and (d), Figs. S5 (e) and (f), Figs. S5 (g) and (h), and Figs. S5 (i) and (j), MSP-SVMsub, 2D-MSSP and MSPM have all produced better visual results on the uncorrected dataset. Overall, MSPM has successfully and accurately classified most of the boundaries in the uncorrected Salinas dataset using a small number of training samples as shown in Fig. S5 (i), which are consistent with the quantitative results given in Table V.

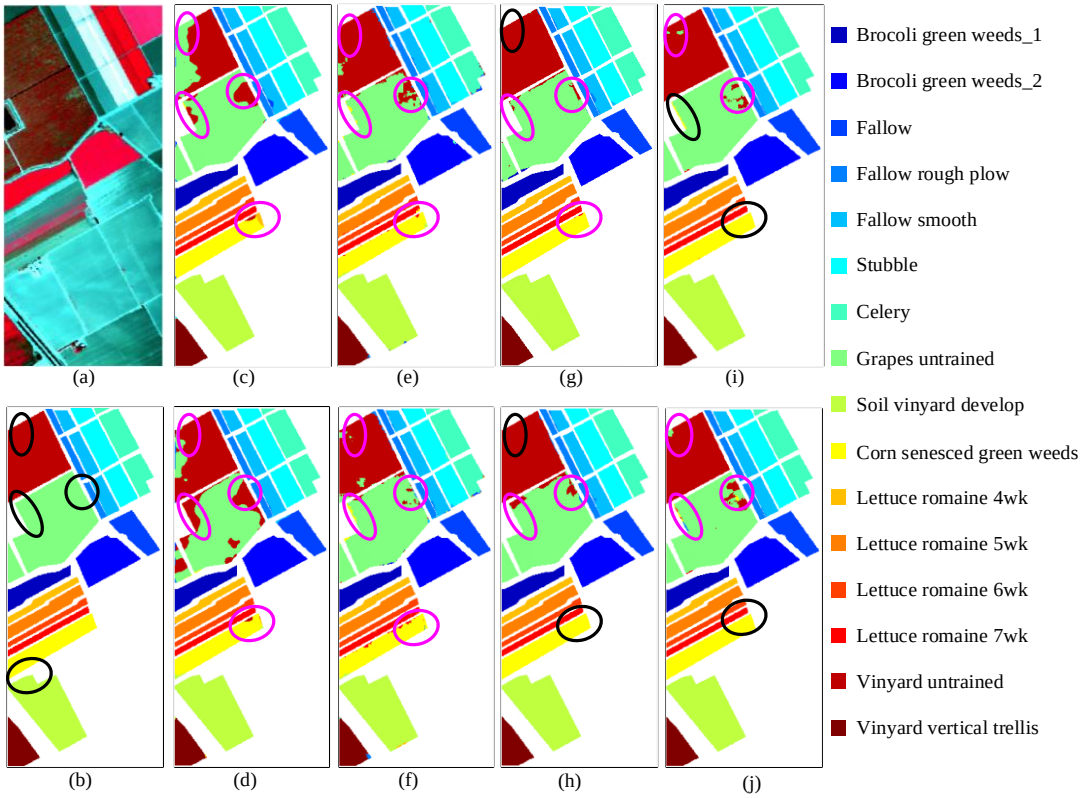

Fig. S5. Classification maps on the Salinas dataset (20 samples per class): (a) False colour image (R: 831nm, G: 657nm, B: 557nm), (b) Ground truth in 16 classes, (c) SMLR-SpATV on uncorrected data, (d) SMLR-SpATV on corrected data, (e) MSP-SVMsub on uncorrected data, (f) MSP-SVMsub on corrected data, (g) 2D-MSSP on uncorrected data, (h) 2D-MSSP on corrected data, (i) MSPM on uncorrected data and (j) MSPM on corrected data.

Visual comparison of the classification maps from our MSPM and other comparing methods on the corrected PaviaU dataset are shown in Fig. S6, where black and magenta circles denote correct and incorrect classified pixels. As seen in Figs. S6 (c)-(j), *Meadows* are severely confused with *Trees* or *Bare Soil* when appearing densely or sparsely visually. By combining spatial features in SS-LRR, FS^{2}LRL and SMLR-SpATV, the noisy estimations of SVM-spe and 2D-EMD are dramatically reduced, and most of the remaining misclassified pixels are further corrected by MSP-SVMsub, 2D-MSSP and MSPM as highlighted in black circles in Figs. S6 (f), (i) and (j). These have also validated by the corresponding higher accuracy values on *Meadows* and *Trees* in Table VI. To differ between *Self-Blocking Bricks* and *Gravel*, only MSPM and 2D-MSSP can discriminate these two to some extent as shown by the black circles in the Figs. S6 (i) and (j) and also the quantitative results in Table VI. These are mainly owing to the multiscale strategies adopted in extraction of spatial and spectral features. The two classes, *Asphalt* and *Trees*, have mixed spectra of surrounding pixels. There are distinct misclassifications in the edge part of *Asphalt* in the maps of MSP-SVMsub and 2D-MSSP, see in magenta circles in Figs. S6 (f) and (i), while other methods have correct classifications. To sum up, the proposed MSPM method obtain the best results in the visual comparison.

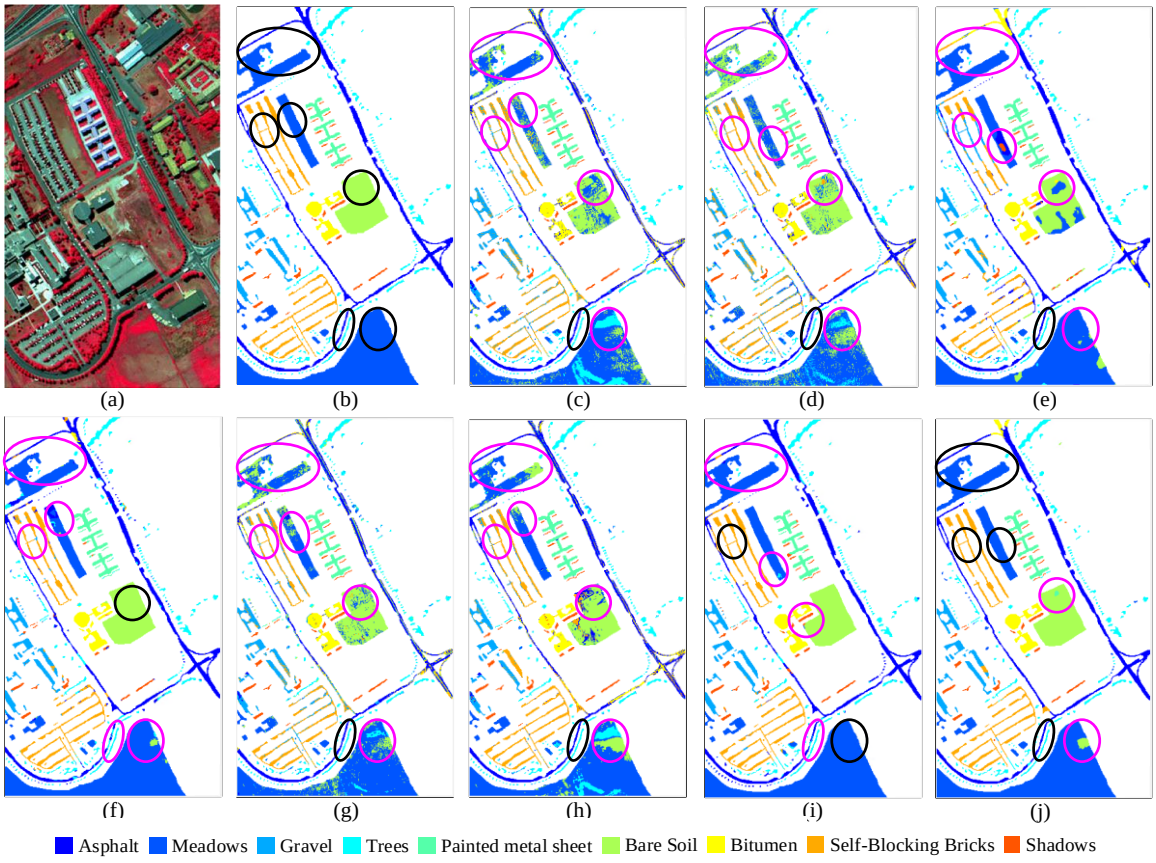

Fig. S6. Classification maps on the corrected PaviaU data (20 samples per class): (a) False colour image (R: 834nm, G: 650nm, B: 550nm), (b) Ground truth with 9 classes, (c) SVM-spe, (d) 2D-EMD, (e) SMLR-SpATV, (f) MSP-SVMsub, (g) SS-LRR, (h) FS2LRL, (i) 2D-MSSP and (j) Our proposed MSPM.

Tables

Here the ablation experiment is carried out to compare the effectiveness of different components within the proposed approach. First, the approach to apply the SVM classifier on the raw spectral profiles of HSI for classification is denoted as SVM-spe. Second, SP-SVM is used to denote SVM based classification of superpixelwise segmented HSI. Finally, MSPM is the proposed framework. As seen, the superpixelwise segmentation has dramatically improved the classification accuracy than SVM-spe which uses only the spectral features. With the proposed Prophet model, the classification accuracy is further improved, especially for Indian Pines and PaviaU datasets. Also, it is worth noting that MSPM has helped to produce higher classification accuracy on the uncorrected datasets than those from the corrected datasets, indicating its unique value in noise-robust classification of HSI even without filtering the water-absorption bands.

The superpixelwise segmentation is one of the key elements to significantly improve the classification accuracy, due mainly to the introduced spatial information whilst suppressing the intra-class variations. However, the Prophet model has also contributed noticeably to the classification, especially to the uncorrected datasets, owing mainly to the strong capability in modelling and prediction in the spectral domain. In other words, superpixelwise segmentation and the Prophet model can supplement to each other in enhancing the features in the spatial and spectral domains, respectively, where the joint spatial-spectral feature has significantly improved the classification accuracy.

TABLE S1 THE OA (%) AND K (IN PARENTHESES) OF DIFFERENT COMPONENTS IN THE PROPOSED FRAMEWORK UNDER 20 TRAINING SAMPLES PER CLASS FOR THE CORRECTED AND UNCORRECTED HSI DATASETS

Datasets		SVM-spe	SP-SVM	MSPM
Indian Pines	uncorrected	57.22 (0.52)	89.10 (0.88)	95.74 (0.95)
	corrected	63.44 (0.59)	91.81 (0.91)	95.18 (0.95)
Salinas	uncorrected	86.27 (0.85)	98.14 (0.98)	99.16 (0.99)
	corrected	86.38 (0.85)	98.67 (0.99)	98.67 (0.99)
PaviaU	corrected	77.15 (0.71)	91.13 (0.90)	97.12 (0.96)

As the uncorrected PaviaU dataset which contains the water absorption bands is unavailable, it is not easy to simulate the true water absorption conditions for an HSI. Although different types of noises can be added to clean HSI datasets, the simulated noise is much different from the water absorption effect [r1, r2]. However, following the practice in [r2], the noisy PaviaU dataset is produced by adding the zero-mean Gaussian noise $N(0,\sigma^2)$ with σ=0.05 to all bands. As shown in Table S2, all comparing methods have worse classification results than those on the corrected dataset, as the introduced Gaussian noise has degraded the extracted features. However, SVM-spe, 2D-EMD, and FS2LRL are more significantly affected by the simulated noise than 2D-MSSP, MSP-SVMsub and the proposed MSPM, where our approach has actually achieved the best results compared to all others. This has validated again the noise-robustness of our MSPM approach. This experiment is added in the updated Supplementary Materials.

TABLE S2 THE OA (%) AND K (IN PARENTHESES) OF DIFFERENT METHODS UNDER VARIOUS NUMBERS OF TRAINING SAMPLES FOR THE CORRECTED AND SIMULATED NOISY PAVIAU DATASET.

Training Samples	Dataset	SVM-spe	2D-EMD	SMLR-SpATV	MSP-SVMsub	SS-LRR	FS^{2}LRL	2D-MSSP	MSPM
5	Noisy	54.84 (0.45)	55.56 (0.45)	66.87 (0.59)	64.33 (0.57)	56.33 (0.46)	54.38 (0.44)	86.89 (0.83)	**88.96 (0.86)**
	Corrected	63.79 (0.55)	63.76 (0.55)	68.02 (0.60)	66.26 (0.59)	63.21 (0.55)	65.86 (0.58)	87.66 (0.84)	**89.43 (0.86)**
10	Noisy	63.25 (0.54)	63.76 (0.55)	75.18 (0.68)	82.53 (0.78)	56.33 (0.55)	64.57 (0.56)	90.02(0.88)	**95.70 (0.94)**
	Corrected	71.42 (0.64)	71.41 (0.64)	78.03 (0.72)	82.65 (0.78)	73.62 (0.67)	78.55 (0.73)	90.66 (0.88)	**95.74 (0.94)**
20	Noisy	69.39 (0.62)	68.90 (0.65)	81.59 (0.76)	92.17 (0.88)	75.42 (0.69)	72.10 (0.65)	96.41(0.95)	**97.00 (0.96)**
	Corrected	77.15 (0.71)	78.41 (0.72)	85.88 (0.82)	92.19 (0.90)	79.26 (0.74)	85.83 (0.82)	96.49 (0.95)	**97.12 (0.96)**

References

[r1] F. Fan, Y. Ma, C. Li, *et al*., "Hyperspectral image denoising with superpixel segmentation and low-rank representation," *Inf. Sci.*, vol. 397, pp. 48-68, Aug. 2017.

[r2] Z. Yue, D. Meng, Y. Sun, *et a*l., "Hyperspectral image restoration under complex multi-band noises," *Remote Sens.*, vol. 10, no. 10, pp. 1631, Oct. 2018.